

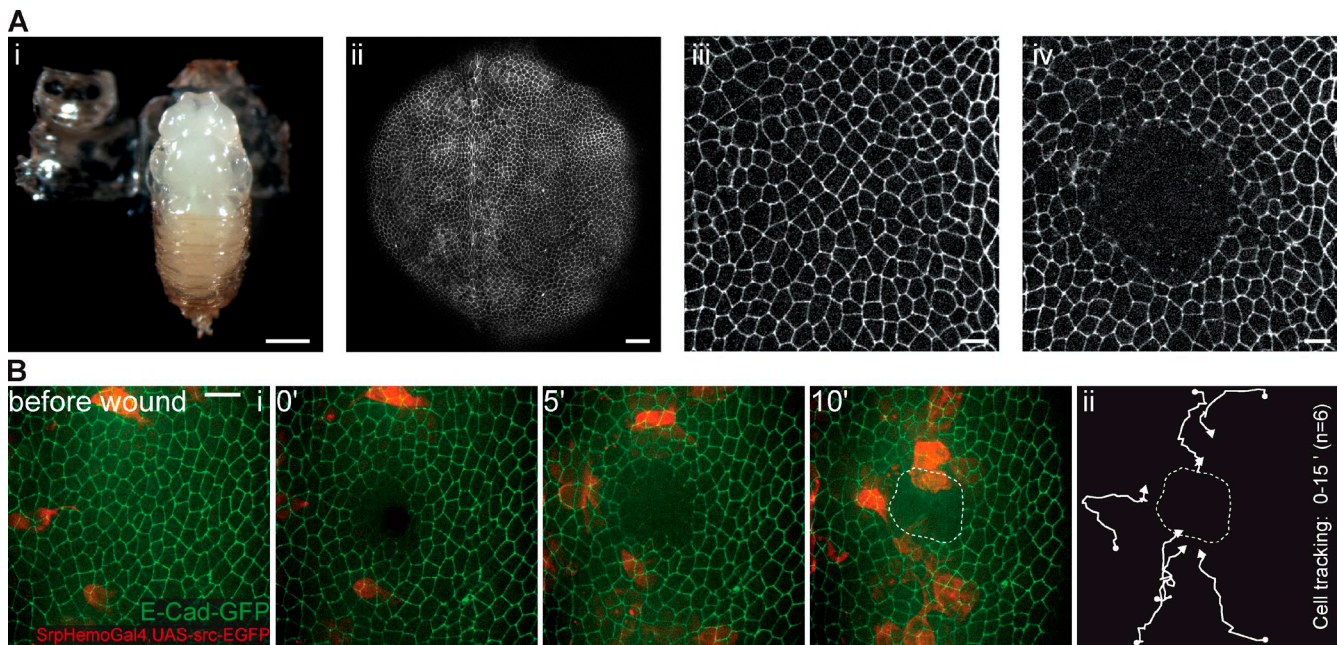
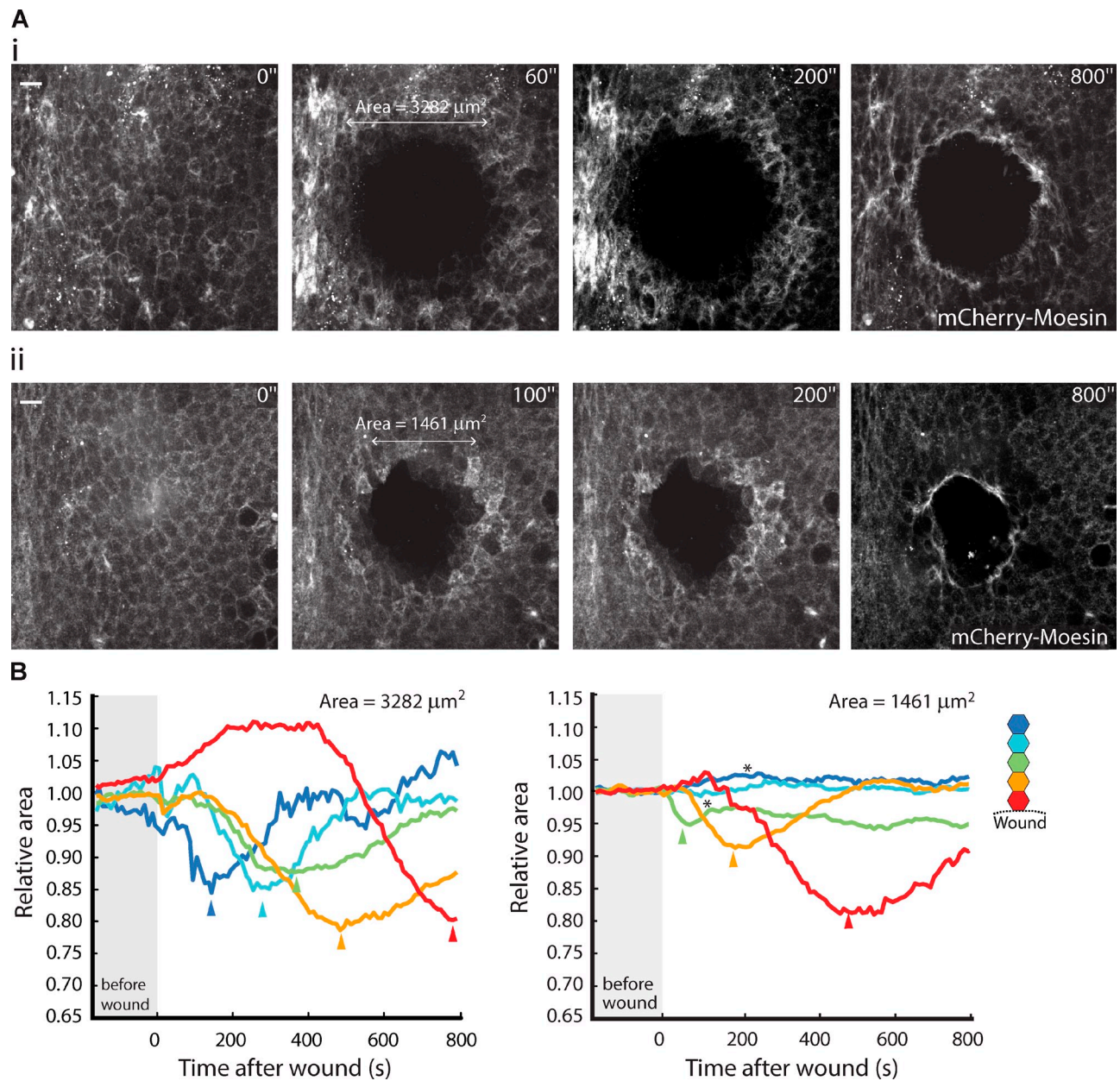
Antunes et al., <http://www.jcb.org/cgi/content/full/jcb.201211039/DC1>

Figure S1. **Pupal wound healing response.** (Ai) Image of a dissected pupa (13 h APF) exposing the notum epithelium. (Aii–Aiv) Different magnifications of a notum expressing E-cadherin–GFP before (ii and iii) and after (iv) wounding. Bars: (i) 0.5 mm; (ii) 40 μ m; (iii and iv) 10 μ m. (Bi) Movie stills of a pupal notum expressing E-cadherin–GFP and UAS-Src-EGFP under the control of the hemocyte-specific driver *SrpHemo-GAL4*. Src-EGFP signal from the basal planes was labeled in a pseudocolor (red) for illustrative purposes. After ablation, hemocytes start to migrate toward the wound and populate the wound region by 10 min after wounding. (Bii) Tracking of hemocytes in the first 15 min after wounding shows oriented hemocyte migration toward the wound. Bar, 40 μ m.



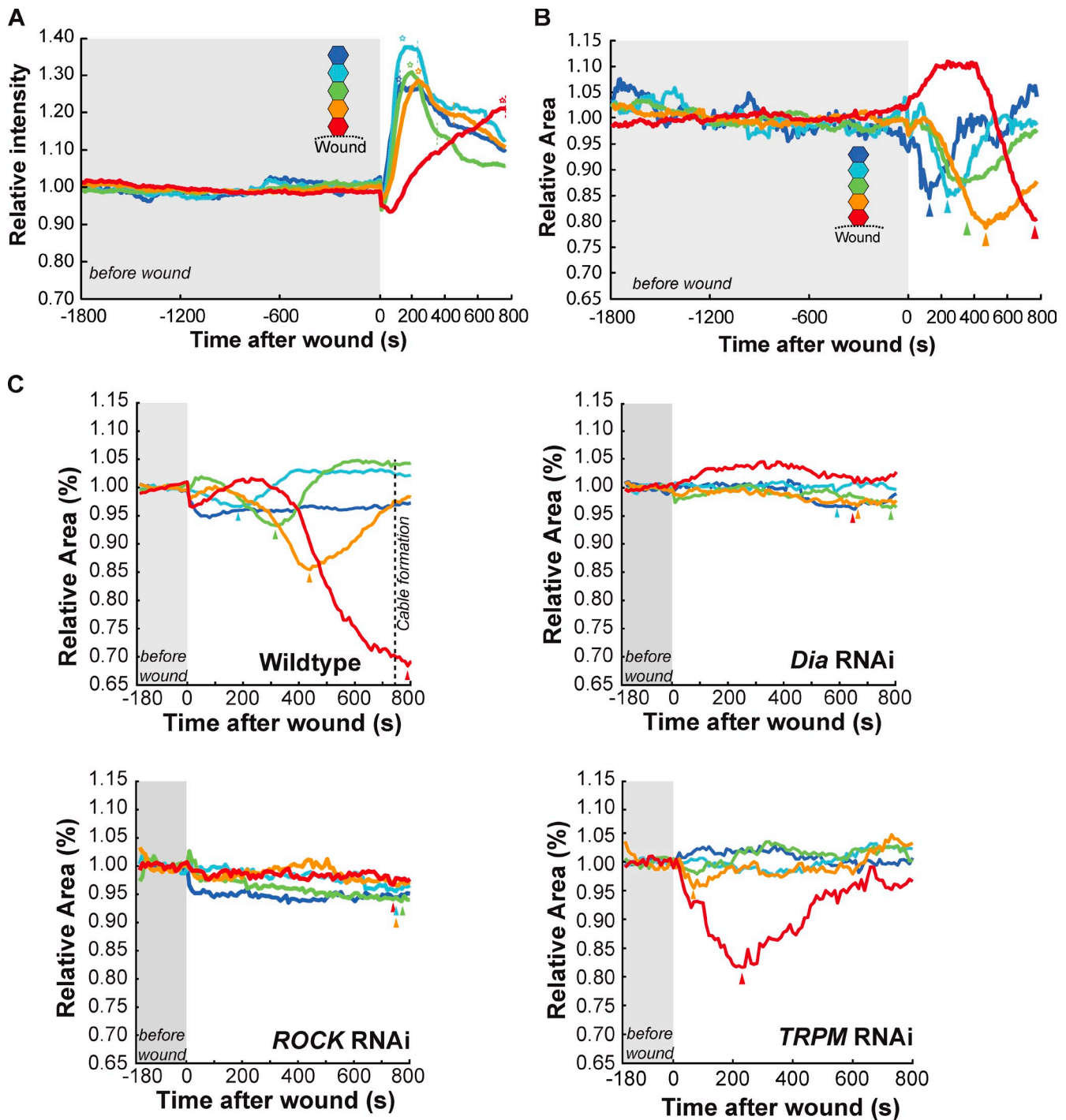


Figure S3. **Actin flow and wave of apical cell constriction are caused by the wound and can be impaired by Dia, ROCK, and TRPM down-regulation.** (A) Graph representing the variation of actin intensity with time before and during the initial stages of wound healing. The actin flow is not detected in the unwounded tissue but can be observed immediately after wounding. Asterisks highlight maximum actin concentration of each cell row revealing that cells closer to the wound reach their maximum actin concentration later. Corresponding time-points of minimum area/maximum contraction are marked with a dashed line. Color code corresponds to Fig. 3 Aii. (B) Graph representing changes in relative cell area during time in a notum expressing E-cadherin-GFP and mCherry-Moesin before and during the initial stages of wound healing. Analysis of cell area for a long period of time before wounding shows that the characteristic wave of cell constriction is not detected during this phase, indicating that this process constitutes a direct tissue response to the wound. Arrowheads highlight maximum constriction of each cell row revealing that cells closer to the wound center contract later. Color code represents distance to the wound according to Fig. 3 Aii. (C) Graphs representing changes in relative cell area during the initial stages of wound healing in WT, Dia, ROCK, and TRPM RNAi. Arrowheads highlight maximum constriction of each cell row revealing that cells closer to the wound center constrict later in WT tissue. Dia, ROCK, and TRPM down-regulation reduces dramatically the contraction flow. Color code corresponds to Fig. 3 Aii.

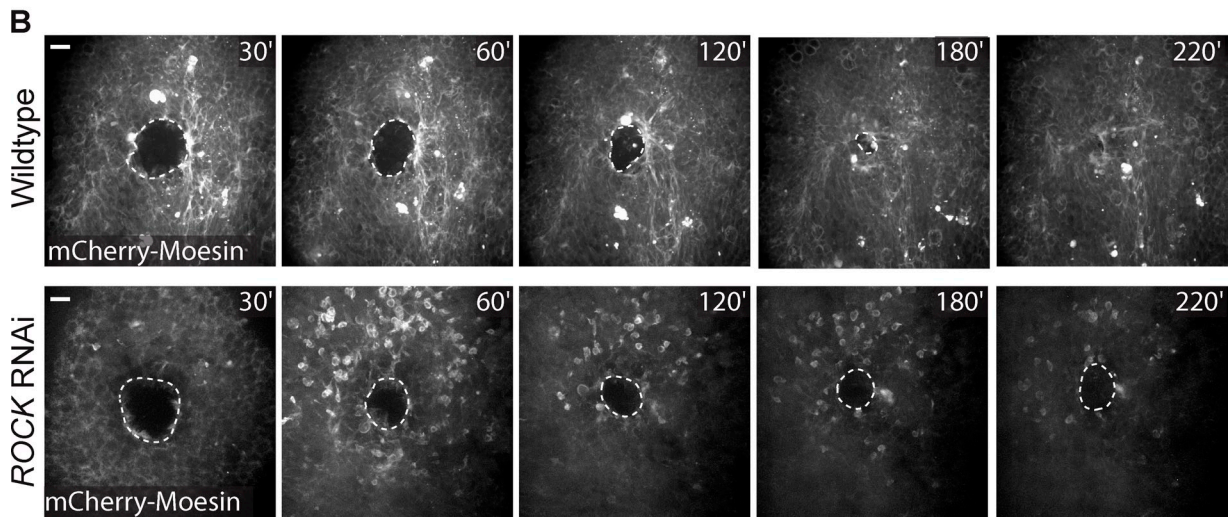
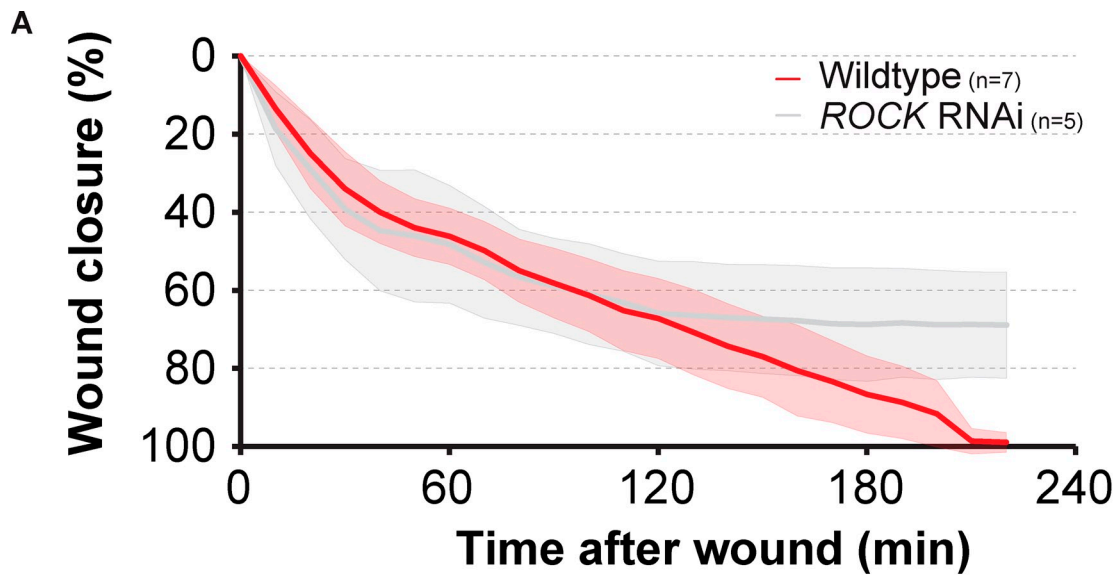


Figure S4. **Wound closure in wild-type and ROCK RNAi.** (A) Graph representing wound closure in wild-type and ROCK RNAi. Wild-type wounds close in ~ 3 h, whereas wounds in ROCK down-regulation do not close. (B) Movie stills showing progress of wound closure in wild-type and ROCK RNAi. After 220 min the wild-type wound has closed, whereas the wound in ROCK down-regulation remains open. Bar, 10 μ m.

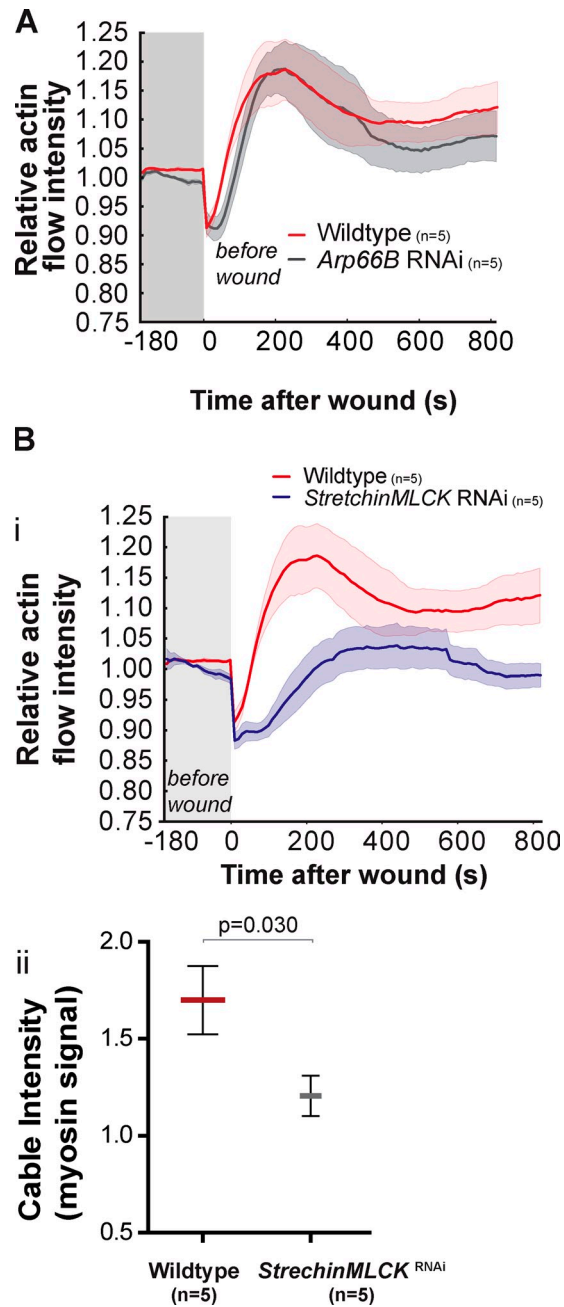
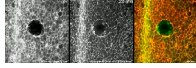
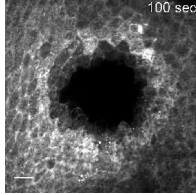


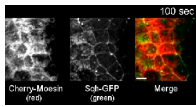
Figure S5. **Stretchin-MLCK but not Arp66B regulates the actin flow.** (A) Graph representing the variation of actin flow intensity in wild-type and Arp66B RNAi. Arp66B down-regulation has no impact on the actin flow, indicating that it does not depend on branched actin polymerization. (Bi) Graph representing the variation of actin flow intensity in wild-type and Stretchin-MLCK RNAi. Stretchin-MLCK knockdown leads to a decrease on the actin flow, indicating that phosphorylation of MLC is necessary for the actin flow formation. (Bii) Quantification of myosin cable intensity after wounding in wild-type and Stretchin-MLCK RNAi-expressing tissues reveals that the cable is weaker upon Stretchin-MLCK down-regulation (P = 0.030, Mann-Whitney test).



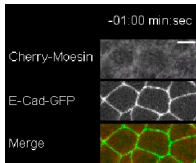
Video 1. **Wound closure in a wild-type epithelium.** Notum epithelium expressing mCherry-Moesin (left, red in merged image) and Spaghetti-Squash-GFP (center, green in merged image) labeling actin and myosin, respectively, highlights wound closure dynamics over 3 h. Merged channels are shown in the right panel. Images were acquired using a spinning disk imaging system (Revolution XD; Andor Technology). Frames were taken every 1 min. Bar, 40 μ m.



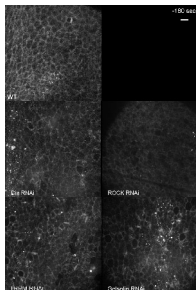
Video 2. **Early tissue response to wounding.** Pupal notum expressing mCherry-Moesin shows the actin flow after wounding. Images were acquired using a spinning disk imaging system (Revolution XD; Andor Technology). Frames were taken every 10 s. Bar, 10 μ m.



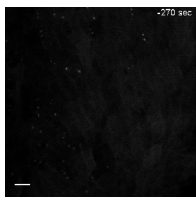
Video 3. **Actomyosin flow culminates in cable formation at the wound margin.** Wounded epithelium expressing mCherry-Moesin (left, red in merged image) and Sqh-GFP (center, green in merged image) labeling actin and myosin, respectively. Merged channels are shown in the right panel. Images were acquired using a spinning disk imaging system (Revolution XD; Andor Technology). Frames were taken every 10 s. Bar, 5 μ m.



Video 4. **Actomyosin flow is the driving force for apical cell constriction wave.** Wound induced in an epithelium expressing mCherry-Moesin (top, red in merged image) and E-cadherin-GFP (center, green in merged image) labeling actin and adherens junctions, respectively. Merged channels are shown in the right panel. Images were acquired using a spinning disk imaging system (Revolution XD; Andor Technology). Frames were taken every 10 s. Bar, 5 μ m.



Video 5. **Actin flow impairment upon Dia, ROCK, TRPM, and Gelsolin down-regulation.** Pupal notum expressing mCherry-Moesin shows the actin flow after wounding in several genetic backgrounds. Dia, ROCK, TRPM, and Gelsolin knockdowns impair the actin flow. Images were acquired using a spinning disk imaging system (Revolution XD; Andor Technology). Frames were taken every 10 s. Bar, 10 μ m.



Video 6. **Calcium dynamics during wound healing.** Notum epithelium expressing G-CaMP3-GFP (Ca^{2+} probe) before and after wounding. Images were acquired using a spinning disk imaging system (Revolution XD; Andor Technology). Frames were taken every 10 s. Bar, 10 μ m.